Theor Chem Acc (2012) 131:1167
DOI 10.1007/s00214-012-1167-1

REGULAR ARTICLE

Validation of a hybrid MD-SCF coarse-grained model for DPPC in non-lamellar phases

Antonio De Nicola · Ying Zhao · Toshihiro Kawakatsu · Danilo Roccatano · Giuseppe Milano

Received: 18 July 2011 / Accepted: 4 December 2011 / Published online: 2 March 2012

Abstract In the framework of a recently developed scheme for a hybrid particle-field simulation technique where self-consistent field theory and molecular dynamics simulation method are combined, specific coarse-grained models for aqueous solutions of phospholipids have been validated. In particular, the transferability of the model in the correct reproduction of non-lamellar phases has been validated against reference particle–particle simulations. By varying the water content, the proposed model is able to correctly describe the different morphologies that are experimentally observed such as micelles and reverse micelles. The lower computational costs of the hybrid techniques allow us to perform simulations of large-scale systems that are needed to investigate the applications of self-assembled structures of lipids in nanotechnologies.

Keywords Coarse-graining · Molecular dynamics · Self-consistent field theory · Lipids

Dedicated to Professor Vincenzo Barone and published as part of the special collection of articles celebrating his 60th birthday.

A. De Nicola · Y. Zhao · G. Milano (✉)
Dipartimento di Chimica e Biologia, Università di Salerno, via Ponte don Melillo, 84084 Fisciano, SA, Italy
e-mail: gmilano@unisa.it

A. De Nicola · G. Milano
IMAST Scarl-Technological District in Polymer and Composite Engineering, P.le Fermi 1, 80055 Portici, NA, Italy

T. Kawakatsu
Department of Physics, Tohoku University, Aoba, Aramaki, Aoba-ku, Sendai 980-8578, Japan

D. Roccatano
Jacobs University Bremen, Campus Ring 1, 28759 Bremen, Germany

1 Introduction

Phospholipids are an important class of compounds having both important biological functions (e.g., cell membranes) and technological applications (e.g., liposomes and micelles).

They can undergo different phase transition in aqueous environments characterized by different morphologies (mesomorphism and polymorphism).

They are an important class of biomolecules because they form lipid bilayer structures that are fundamental building blocks of cellular membranes. For this reason, lipid bilayers have been attracting the interest of computational biophysics community, where people perform atomistic and coarse-grained molecular dynamics simulations of these systems for long time [1–13].

Mesomorphism and polymorphism can occur when lipids are not included in the cell biomembranes. Despite their importance in the biological systems, the molecular structures of biological cell membranes, especially the structures of ion channels and transmembrane proteins, are not well understood yet.

When phospholipids are no longer under the constraints that are imposed by intermolecular interactions that are present within the biomembrane, they can form non-lamellar (non-bilayer) phases, where the non-lamellar phases include the hexagonal and cubic phases as well as the diluted micellar phases.

Hexagonal phases are characterized by tubular aggregates, and they can be composed of either normal or reverse aggregates. Cubic phases are composed of curved bilayers or micelles. Depending on the water concentration, micelles change their aggregation form from normal ('oil in water') to reverse ('water in oil') micelles.

Due to their relevance to the biological systems, most of the simulation works on lipids have been focused on the bilayer phase [10, 14–17]. With the advent of nanotechnology, self-assembled structures of lipids started to be exploited in different ways. Lipids can be used as templates for the assembly of nanoparticles. For example, gold nanoparticles can be prepared using templates formed by the tubular nanodomains of lipids [18, 19]. Lipid micelles can be used as dispersant for carbon nanotubes in aqueous media [20]. Liposomes can be used for drug delivery [21] and as nanoreactors [22]. Reverse micelles can be used as templates for the nanofabrication of tubes of conductive polymers [23].

Although atomistic simulations can provide very detailed and chemically consistent models of biological phospholipids, they are very expensive way of studying the assembling processes involving nanomaterials occurring on the mesoscopic time (>μs) and length scales (>100 nm).

In order to bridge this gap between the length and time scales covered by the atomistic simulations and the actual scales of the relevant phenomena, different types of coarse-grained (CG) models have been developed for phospholipids. For example, implicit solvent models and explicit solvent models for lipid bilayers have been reported [24–26]. Among different approaches for developing such CG models, specific models that retain some chemical details are useful in determining the connection between the chemical structure on the atomistic scales and the nanostructures that are obtained by self-assembly in different conditions.

In particular, these CG models usually employ several different types of beads (not just hydrophobic and hydrophilic), with several parameters for the force fields derived from simulations based on atomistic models. A successful and very widely explored example of this approach is the MARTINI CG model developed by Marrink and co-workers [27]. In the MARTINI force field, the phospholipids are described by several types of beads interacting via Lennard–Jones-type potentials with different interaction parameters, with which one can describe a smooth variation from the hydrophobic to hydrophilic characters. Despite its simplicity, the MARTINI force field is able to reproduce with surprisingly good accuracy the properties of the self-assembly of lipid molecules in the bilayers and the micellar phases [15, 28, 29].

A different coarse-graining approach is based on a field representation and has been proposed to model soft matter systems. In particular, in the framework of the self-consistent field (SCF) theory, the model systems are not represented by particles but by density fields and the mutual interactions between segments (beads) are decoupled and replaced by interactions with static external fields [30]. Numerous applications of this approach to block copolymers [31–35], proteins [36], polymer composites [37] and colloidal particles [38, 39] for studying the large-scale phenomena in soft matter have been proposed. There have been several approaches to phospholipids and water mixtures using approaches based on the field descriptions [34, 40–43].

More recently, Müller and Smith [44] introduced a hybrid approach in the framework of SCF theory by combining it with a Monte Carlo simulation of a coarse-grained model of polymer chains to study the phase separation in binary polymer mixtures. This approach has been widely and successfully applied by Daoulas et al. [45] to coarse-grained models of diblock copolymer thin films and by Detcheverry et al. [46, 47] to polymer nanocomposites. One of the advantages of this hybrid approach is the absence of any limitation in treating complex molecular architectures and/or intramolecular interactions. With these preceding studies, very recently, a hybrid particle-field approach, where the molecular dynamics (MD) simulation method is combined with SCF description (MD-SCF), was proposed and an implementation suitable for the treatment of atomistic force fields and/or specific coarse-grained models has been reported [48, 49]. In particular, specific coarse-grained models for phospholipids and water, suitable for MD-SCF simulations, have been developed. These models and the set of parameters needed to evaluate the interactions between the particles and the density fields have been optimized to reproduce structural properties of reference full-atomistic MD simulations of lipid bilayers. It was also proved that this MD-SCF model is able to reproduce correctly the physical behavior of the lipid bilayers [50]. The aim of the present study was to validate these models for non-bilayer phases. In particular, the transferability of the model to systems different water contents has been validated against reference simulations.

The paper is organized as follows: in Sect. 2, we describe the basic concept of the SCF theory, which is useful for the reader to understand the present investigation. We also give a brief description of the computational scheme for the hybrid particle-field MD-SCF simulations. In Sect. 3, the validation of the model by comparison with classical MD simulations using the MARTINI force field is reported. In the following, these full-atomistic simulations will be referred as particle–particle (PP) simulations. Finally, simulation results on the non-lamellar-type self-assembly of dipalmitoylphosphatidylcholine (DPPC) molecules in its aqueous solutions with various concentrations are shown.

2 Computational methods

2.1 MD-SCF theory and implementation

In this section, a brief exposition of the recently developed hybrid MD-SCF simulation scheme is reported. This section is intended to quickly guide the reader to get the basis of the methodology and to understand the framework of the present investigation. In order to obtain this approach in more detail, the readers should refer to Ref. [48] where the complete derivation and the implementation are described and to references [30, 33, 51–53] for general reviews of SCF methods.

The main feature of the hybrid MD-SCF approach is that the evaluation of the non-bonded force and its potential between atoms of different molecules, that is, the most computationally expensive part of MD simulations, can be replaced by the evaluation of an external potential that is dependent on the local density at position $\mathbf{r}$ in MD-SCF simulations. According to the spirit of SCF theory, a many body problem like molecular motion in many molecule systems is reduced into the problem of deriving the partition function of a single molecule in an external potential $V(\mathbf{r})$. Then, non-bonded force between atoms of different molecules can be obtained from a suitable expression of the $V(\mathbf{r})$ and its derivatives.

In the frame of SCF theory, a molecule is regarded to be interacting with the surrounding molecules not directly but through a mean field. To derive such a mean field picture, we start from a Hamiltonian of a system that is composed of M molecules. The Hamiltonian is split into two parts $\hat{H}(\Gamma) = \hat{H}_0(\Gamma) + \hat{W}(\Gamma)$, where Γ specifies a point in the phase space, which is used as shorthand for a set of positions of all atoms in the system. Here and also in the following, the symbol ^ (hat) indicates that the associated physical quantity is a function of the microscopic states described by the phase space Γ.

$\hat{H}_0(\Gamma)$ is the Hamiltonian of a reference ideal system composed of non-interacting chains but with all the intramolecular interaction terms (bond, angle and non-bonded interactions) that are taken into account in the standard MD simulations. The term $\hat{W}(\Gamma)$ is the deviation from the reference system and taking into account of the intermolecular non-bonded interactions.

Assuming the canonical (NVT) ensemble, the partition function of this system is given by the following equation:

$$Z = \frac{1}{M!}\int d\Gamma \exp\left\{-\beta[\hat{H}_0(\Gamma) + \hat{W}(\Gamma)]\right\}, \tag{1}$$

where $\beta = \frac{1}{k_B T}$.

From a microscopic point of view, the number density of segments is defined as a sum of delta functions placed at the center of mass of each segment as [30, 54]

$$\hat{\phi}(\mathbf{r};\Gamma) = \sum_{p=1}^{M}\sum_{i=0}^{S(p)} \delta\left(\mathbf{r} - \mathbf{r}_i^{(p)}\right), \tag{2}$$

where M is the total number of molecules in the system, $S(p)$ is the number of particles contained in pth molecule, and $\mathbf{r}_i^{(p)}$ is the position of the ith particle in pth molecule. The deviation $\hat{W}(\Gamma)$, according to Eq. 1, from the reference state $\hat{H}_0$ originates from the interactions between molecules. Several assumptions are introduced to calculate the interaction term $\hat{W}(\Gamma)$. First of all, we assume that $\hat{W}(\Gamma)$ depends on Γ only through the segment number density $\hat{\phi}(\mathbf{r};\Gamma)$ as

$$\hat{W}(\Gamma) = W[\hat{\phi}(\mathbf{r};\Gamma)], \tag{3}$$

where $W[\hat{\phi}(\mathbf{r};\Gamma)]$ means that W is a functional of $\hat{\phi}(\mathbf{r};\Gamma)$. Using the identity for the δ-functional

$$\delta[\hat{\phi}(\mathbf{r};\Gamma) - \phi(\mathbf{r})] = \int D\{w(\mathbf{r})\}\exp\left[i\int w(\mathbf{r})\left\{\hat{\phi}(\mathbf{r};\Gamma) - \phi(\mathbf{r})\right\}d\mathbf{r}\right],$$

we can rewrite the partition function in Eq. 1 as

$$Z = \frac{1}{M!}\int D\{\phi(\mathbf{r})\}\int D\{w(\mathbf{r})\}\exp\left\{-\beta\left[-\frac{M}{\beta}\ln z + W[\phi(\mathbf{r})] - \frac{1}{i\beta}\int w(\mathbf{r})\phi(\mathbf{r})d\mathbf{r}\right]\right\}, \tag{4}$$

where z is the single-molecule partition function, and $w(\mathbf{r})$ is a conjugate field of $\phi(\mathbf{r})$ which appeared in the Fourier representation of the δ-functional, and is a complex field [53].

For evaluating this partition function approximately, the integrals over $\phi(\mathbf{r})$ and $w(\mathbf{r})$ in Eq. 4 are replaced with a Gaussian integral around the most probable state that minimizes the argument of the exponential function on the right side of Eq. 4 (so-called saddle point approximation).

The minimization conditions in the form of functional derivatives result in

$$\begin{cases} V(\mathbf{r}) \equiv \frac{1}{i\beta}w(\mathbf{r}) = \frac{\delta W[\phi(\mathbf{r})]}{\delta\phi(\mathbf{r})} \\ \phi(\mathbf{r}) = -\frac{M}{\beta z}\frac{\delta z}{\delta V(\mathbf{r})} = \left\langle\hat{\phi}(\mathbf{r};\Gamma)\right\rangle, \end{cases} \tag{5}$$

where $\phi(\mathbf{r})$ is the coarse-grained density at position $\mathbf{r}$ and $V(\mathbf{r})$ is the external potential conjugate to $\phi(\mathbf{r})$ which is a real field now.

In term of Eq. 5, it is possible to acquire an expression for a density-dependent external potential acting on each segment.

Next, we assume that the density-dependent interaction potential W, where each component species is specified by the index K, takes the following form:

$$W[\{\phi_K(\mathbf{r})\}] = \int \mathrm{d}\mathbf{r}\left(\frac{k_BT}{2}\sum_{KK'}\chi_{KK'}\phi_K(\mathbf{r})\phi_{K'}(\mathbf{r}) + \frac{1}{2\kappa}\left(\sum_K \phi_K(\mathbf{r}) - 1\right)^2\right), \quad (6)$$

where $\phi_K(\mathbf{r})$ is the coarse-grained density of the species K at position $\mathbf{r}$ and $\chi_{KK'}$ are the mean field parameters for the interaction of a particle of type K with the density fields due to the particles of type K'. Here, we redefined $\phi_K(\mathbf{r})$ as the number density of the species K normalized by the total average number density of the segments. This change in the definition of $\phi_K(\mathbf{r})$ only affects the scale of the conjugate field $V(\mathbf{r})$.

The second term of the integrand on the right-hand side of Eq. 6 is the relaxed incompressibility condition, and κ is the compressibility that is assumed to be sufficiently small [54]. Then, the corresponding mean field potential is given by

$$V_K(\mathbf{r}) = \frac{\delta W[\{\phi_K(\mathbf{r})\}]}{\delta\phi_K(\mathbf{r})} = k_BT\sum_{K'}\chi_{KK'}\phi_{K'}(\mathbf{r}) + \frac{1}{\kappa}\left(\sum_K \phi_K(\mathbf{r}) - 1\right). \quad (7)$$

Taking the case of a mixture of two components A and B as an example, the mean field potential acting on a particle of type A at position $\boldsymbol{r}$ is given by

$$V_A(\mathbf{r}) = k_BT[\chi_{AA}\phi_A(\mathbf{r}) + \chi_{AB}\phi_B(\mathbf{r})] + \frac{1}{\kappa}(\phi_A(\mathbf{r}) + \phi_B(\mathbf{r}) - \phi_0). \quad (8)$$

Thus, the force acting on the particle A at position $\mathbf{r}$ imposed by the interaction with the mean field is

$$F_A(\mathbf{r}) = -\frac{\partial V_A(\mathbf{r})}{\partial r} = -k_BT\left(\chi_{AA}\frac{\partial\phi_A(\mathbf{r})}{\partial\mathbf{r}} + \chi_{AB}\frac{\partial\phi_B(\mathbf{r})}{\partial\mathbf{r}}\right) - \frac{1}{\kappa}\left(\frac{\partial\phi_A(\mathbf{r})}{\partial\mathbf{r}} + \frac{\partial\phi_B(\mathbf{r})}{\partial\mathbf{r}}\right). \quad (9)$$

The main advantage of hybrid MD-SCF scheme is that the most computationally expensive part of the MD simulations, that is, the evaluation of the non-bonded force between atoms of different molecules, is replaced by the evaluation of forces between single molecules with an external potential. In order to connect particle and field models, for the proposed hybrid MD-SCF scheme, it is necessary to obtain a smooth coarse-grained density function directly from the particle positions Γ. Let us denote this procedure as

$$\bar{S}\{\hat{\phi}(\mathbf{r};\Gamma)\} = \phi(\mathbf{r}), \quad (10)$$

where $\bar{S}$ is a symbolic name of the mapping from the particle positions to the coarse-grained density. In order to obtain a smooth spatial density from particle positions, the simulation box is divided into several cells. In particular, particles are sorted and, according to their positions, assigned to $ncell = n_xn_yn_z$ (where n_x, n_y and n_z are the number of cells in the x, y and z directions, respectively). Furthermore, according to the position of each particle inside a cell, a fraction of it will be assigned to each vertex of the cell [46, 48–50, 55–57]. In order to explain the procedure, a simpler two-dimensional case is described. In Fig. 1a, the structure of a phospholipid and the corresponding density field is schematized.

As described in Fig. 1b, the fraction of a particle assigned to a given lattice point is proportional to the area of a rectangle shown in the figure. For example, for a particle with coordinates $\underline{x}$ and $\underline{y}$, a fraction $(l - \underline{x})(l - \underline{y})/l^2$ will be assigned to the mesh point 1 and a fraction of $\underline{xy}/l^2$ at mesh point 4 in Fig. 1b (for simplicity, l is the length of the cell in both x and y directions). Thus, the density at every mesh point is the sum of all fractions assigned from all the cells that share a given lattice point. According to the procedure described above, the size of the cell l is a parameter defining the density coarse-graining. Larger is the value of l, more particles will be included in every cell and coarser will be the calculated density. Once the coarse-grained density has been calculated from particle positions, the spatial derivatives of the density field can be evaluated. Spatial derivatives can be obtained by the differentiation of the density lattice. In this way, the lattice where the derivatives are defined is staggered with respect to the lattice where the density is defined. As schematized in Fig. 1b, the squares indicate the lattice points where the density is defined. Correspondingly, the density gradients are defined on the center of each edge (staggered lattice points indicated by crosses in Fig. 1b) of the square surrounding the density lattice points.

Once that both density and derivatives have been computed on their corresponding lattices, the potential energy and forces acting on the particles can be calculated using values obtained by the interpolation of the density and of its spatial derivatives in Eqs. 8 and 9.

The iteration algorithm used in MD-SCF approach is explained in the following. According to the initial configurations of the system (at time t_0), a starting value of the coarse-grained density is obtained, where the coarse-grained density is defined on a lattice and the values of the density and density gradients at the particles positions are

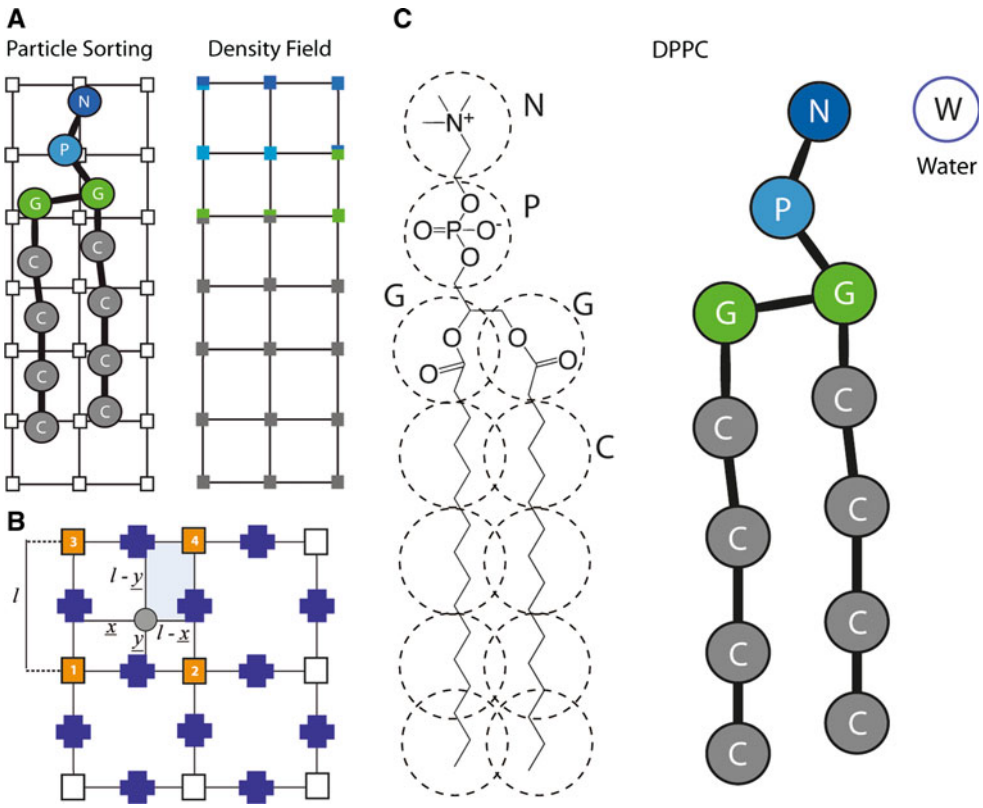

Fig. 1 **a** Construction of coarse-grained density for a phospholipid. **b** Criterion for the assignment of particle fractions to lattice points. **c** Adopted coarse-graining scheme for DPPC

calculated by linear interpolation. Then, from the density gradients, forces acting on the particles at position **r** due to the interaction with the density fields are computed according to Eq. 9. The total force acting on the particles will be the sum of the intramolecular forces (bonds, angles and intramolecular non-bonded forces calculated as in classical MD simulations) and the forces due to the interactions of particles with density fields. After the force calculation, a new configuration will be then obtained by the integration of the equation of motion. In principle, for every new configuration, an update of the CG density calculated from the new coordinates should be performed. Test simulations have shown that, due to the collective nature of the density fields, it is possible to define an update frequency of the coarse-grained densities without the loss of accuracy [48, 49]. These results are in agreement with the concepts behind the quasi-instantaneous field approximation discussed by Daoulas et al. [58] in the framework of Single Chain in Mean Field (SCMF) Monte Carlo simulations.

In other words, the values of the coarse-grained density at lattice points are not updated at every timestep but only at every prefixed density update time (Δt_{update}). Then between two updates, the values of the densities on the lattice used to interpolate both density and its derivatives will be constant. When an update of density is performed, a new coarse-grained density will be obtained and the iteration algorithm converges when the coarse-grained density and the particle-field potential become self-consistent.

2.2 Models and parameters

For the intramolecular interactions, parameters of the coarse-grained (CG) MARTINI model have been considered [59]. In this model, bonds are described by a harmonic-type potential of the form:

$$V_{\text{bond}}(R) = \frac{1}{2} K_{\text{bond}} (R - R_{\text{bond}})^2 \tag{11}$$

where R_{bond} is the equilibrium bond length and K_{bond} is the force constant of the bond. These parameters of the bond potential used in the present study are reported in Table 1.

The stiffness of the chains is also taken into account by a harmonic bending potential $V_{\text{angle}}(\theta)$ that depends on the cosine of the angle θ between two successive bonds.

$$V_{\text{angle}}(\theta) = \frac{1}{2} K_{\text{angle}} \{\cos(\theta) - \cos(\theta_0)\}^2 \tag{12}$$

where K_{angle} is the force constant and θ_0 is the equilibrium bond angle. Angle parameters adopted for the models of this paper are reported in Table 2.

Intramolecular non-bonded interactions are modeled using the parameters of the Lennard–Jones potentials and have been set for all non-bonded pairs $\varepsilon = 2.0$ kJ/mol and

Table 1 Parameters for bonding energetic terms

Bond type	b_o (nm)	K_b (kJ mol^{-1} nm^{-2})
N–P	0.470	1,250
P–G	0.470	1,250
G–G	0.370	1,250
G–C	0.470	1,250
C–C	0.470	1,250

Table 2 Parameters for angle energetic terms

Angle type	θ_o (°)	K_θ (kJ mol^{-1})
P–G–G	120	25.0
P–G–C	180	25.0
G–C–C	180	25.0
C–C–C	180	25.0

Table 3 Particle–field interaction parameters $\chi_{KK'} \times RT$ (kJ/mol) for particles of type K interacting with density fields due to particle of type K' are reported

	N	P	G	C	W
N	0.00	−1.50	6.30	9.00	−8.10
P	−1.50	0.00	4.50	13.50	−3.60
G	6.30	4.50	0.00	6.30	4.50
C	9.00	13.50	6.30	0.00	33.75
W	−8.10	−3.60	4.50	33.75	0.00

$\sigma = 0.47$ nm (which are repulsive according to the MARTINI nomenclature) [59].

Particle-field $\chi_{KK'}$ parameters (Eqs. 6 and 7) needed to calculate the interactions between a particle of type K and the density fields due to the particles of type K' are listed in Table 3. These parameters have been tuned to reproduce structural properties of lipid bilayers. In particular, electron density profiles of reference particle–particle simulations and bilayer thicknesses can be well reproduced for DPPC and several other lipids [50]. Furthermore, in order to determine the value of the parameter κ that regulates the strength of the incompressibility condition imposed in Eq. 7, we analyzed the behavior of density fluctuations in reference PP simulation. More detailed information about the model parameters can be found in Ref. [50].

2.3 Simulations details

For the use of a reference system for the CG simulations, classical PP-MD simulations have been performed using the program GROMACS (ver. 3.3) [60]. The timestep used for the integration of equation of motion was 0.03 ps. The temperature was kept constant using the weak coupling method with $\tau_T = 0.1$ ps, where the target temperatures are listed in Table 3. A cut-off of 1.5 nm has been used to truncate the non-bonded interactions.

The parallel molecular dynamics program OCCAM [61] was used for MD-SCF simulations. MD-SCF simulations have been performed using a timestep of 0.03 ps, with the *NVT* ensemble by keeping the temperature constant using Andersen thermostat with a collision frequency of 5 ps^{-1}.

Details on the systems size and composition used in the simulations in the present study are summarized in Table 4.

3 Results and discussion

3.1 Model validation: PP-MD versus MD-SCF simulations

According to the coarse-graining strategy explained in the previous chapter, pair interactions between particles are replaced by the calculation of the interactions of single particles in an external field. The main parameters regulating these interactions are the mean field parameters $\chi_{KK'}$ describing the interaction between particles of type K with the density fields due to the particles of type K'. As described in the previous chapters, a set of parameters that are able to reproduce structural properties of lipid bilayers for DPPC and several other lipids has been recently reported [50].

In principle, the parameters of a coarse-grained model are not always transferable. For example, χ parameters can be temperature and composition dependent. This dependency cannot be known a priori and needs to be investigated for every coarse-grained model. This feature of coarse-grained models is general and is relevant also for particle–particle coarse-grained models [62].

The main aim of the present paper was to validate the hybrid MD-SCF models proposed for lipid bilayers in non-lamellar phases corresponding to high or low water content.

In this subsection, in order to validate the MD-SCF simulations, the results of MD-SCF simulations are compared with those of the classical PP-MD simulations.

In Fig. 2, self-assemblies of DPPC/water systems simulated using PP and MD-SCF models at two different water contents (systems **1** and **2** of Table 4, respectively) are compared. In the reference PP model, each CG water bead corresponds to 4 real water molecules. In the present article, this factor has been taken into account. For example, ratio between CG water beads and DPPC molecules reported in Table 4 is for systems **1** is 182 and for system **2** is 0.8. In terms of real water molecules, these ratios would be 728 and 3.2.

Table 4 Details about simulated systems

System	Box size (nm)	Composition				T (K)
	$x = y = z$	No. of particles	No. of DPPC	No. of water	Water/DPPC[a] ratio	
1	7.923	3,876	20	3,636	182	325
2	8.176	4,096	320	256	0.8	325
3	12.964	21,216	1,664	1,248	0.75	318
4	13.486	24,128	1,664	4,160	2.5	318
5	12.376	18,600	300	15,000	50	318
6	17.309	42,588	208	40,092	192.7	318

[a] In the reference PP model, each CG water bead corresponds to 4 molecules; in the text of the manuscript and in the figures, this factor has been taken into account

For both of these simulations, the initial configuration and the simulation conditions are the same. The starting configuration used in both simulations is a random mixture of DPPC and water molecules.

For high water concentration (system **1**), in both PP and MD-SCF simulations, the formation of a micelle is observed. In the case of MD-SCF simulation, the self-assembling process of the micelle takes about 15 ns, which is faster than the PP simulation (see Fig. 2a), where the micelle is obtained after 25 ns (see Fig. 2b). In Fig. 3, the radial density profiles of the micelle obtained in the MD-SCF (Fig. 3a) and PP (Fig. 3b) simulations are compared. Radial density profiles obtained in the MD-SCF and PP simulations are similar. The main difference is observed in the slopes of the curves. A further validation of the proposed MD-SCF models can be done by calculating the average number of lipid per micelle. These calculations can be reliable only using larger systems in which two or more micelles are in equilibrium with free lipid molecules. These results will be discussed in Sect. 3.3.

The system at low water concentration (system **2**) shows a different behavior; in both PP and MD-SCF simulations, a formation of reverse micelles is observed. In particular, from Fig. 2c, it is clear that at about 12 ns the system reaches a stable reverse micellar phase. In this reverse micellar phase, polar head groups of the lipids and the water molecules form cylinders included in the hydrophobic majority phase made of lipid tails. This result is in agreement with the formation of a hexagonal reverse-cylindrical phase. The formation of this phase structure is more clearly observed in Fig. 4a where structures obtained from MD-SCF and PP simulations are compared.

Differently from MD-SCF simulations, the cylinders obtained in the PP simulation are less regular and the water beads are not included in the cylinders but they form clusters with different sizes inside the hydrophobic phase formed by the lipid tails. We expect that, in this case, the simulated system is "trapped" in a metastable phase and the slower dynamics of PP simulations does not allow the system to escape from such a metastable phase to become more stable hexagonal structure. In order to confirm this point, the equilibrium structure obtained in the MD-SCF simulation is used as the initial state for the PP simulation after a short energy minimization is performed. In this case, as shown in Fig. 4b, the non-bonded interaction energy is lower and the structure is stable during all the simulations. In Fig. 4c, this structure is depicted in a view showing the hexagonal arrangement.

3.2 Effects of density coarse-graining on structure and dynamics

As described in Sect. 2, coarse-grained density fields $\phi_K(\mathbf{r})$, obtained from the particle positions for every particle type K, are used to calculate MD-SCF potentials and forces using Eqs. 8 and 9.

According to the scheme described in Sect. 2, two parameters, that is, the cell size l and the update frequency Δt_{update}, regulate the degree of coarse-graining of the density fields. Larger cell sizes lead to more collective density fields. As for the value of the update frequency, it has to be chosen in a way that the approximation of slow variation in the field with respect to the displacements of the particles is valid between two density updates. As already pointed out by Daoulas et al. in the context of SCMF Monte Carlo simulations, the update of the density field introduces the correlations between different molecules. On the other side, in the timesteps between two updates, the molecules are decoupled and move independently in the external density field. The validity of the so-called *quasi-instantaneous field approximation* [58] will be considered in the following by comparing simulation results using different update frequencies. It is worth to note that the concept of using different time-integration steps for "stiff" and "soft" degrees of freedom has been exploited also for PP simulations. Popular examples of this can be Molecular Dynamics algorithms with multiple time scales [63].

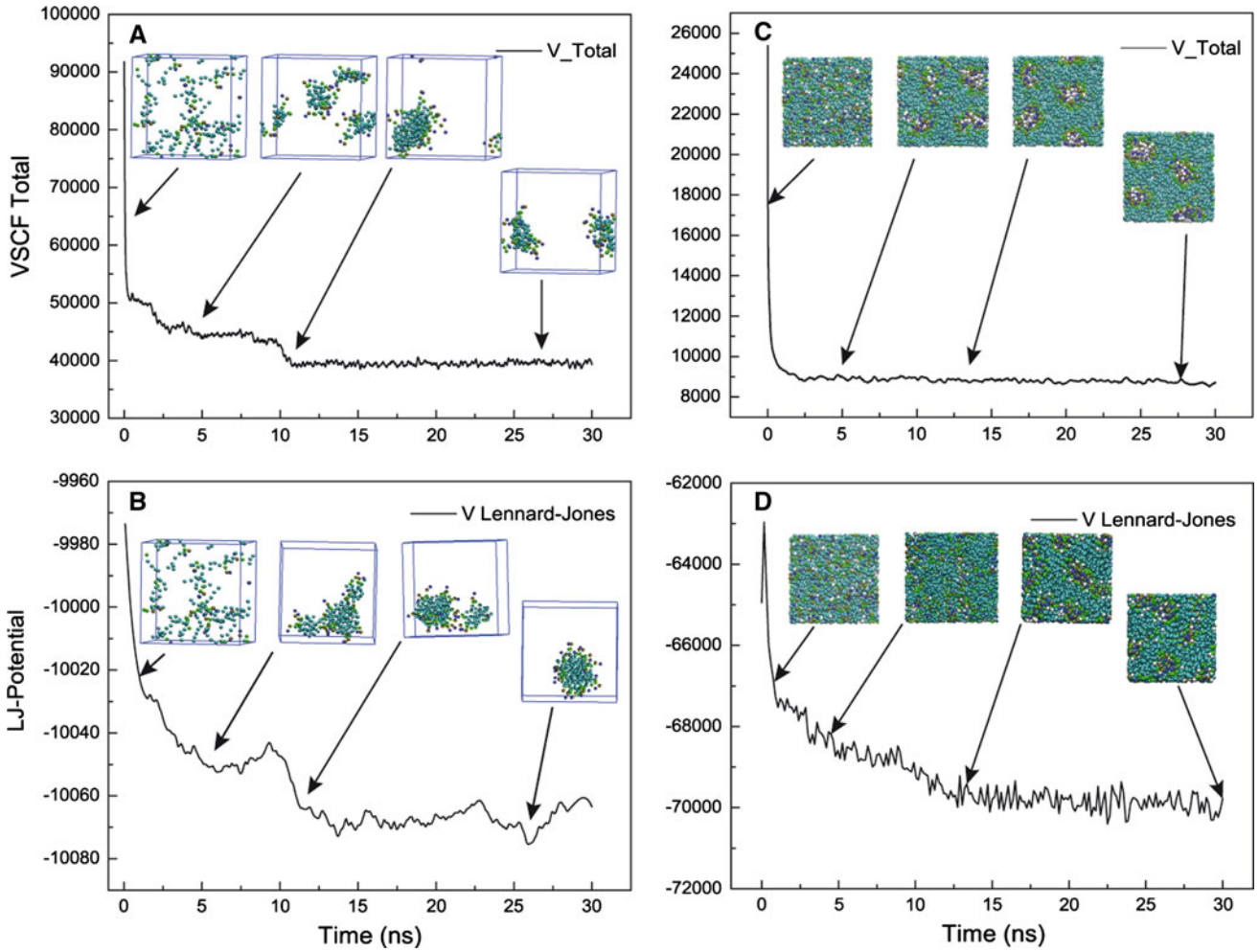

Fig. 2 Comparison of the self-assembling process of a DPPC micelle in water for MD-SCF (**a**) and PP simulations (**b**). Comparison of self-assembling process of a reverse micellar phase for MD-SCF (**c**) and PP simulations (**d**) is given. In the figures, the time behavior of particle-field intermolecular potential in the MD-SCF simulation is compared with the behavior of the non-bonded Lennard–Jones potential in the PP-MD simulation. Potential units are kJ/mol

In Fig. 5, the structures obtained using different density update frequencies and cell sizes are summarized. In particular, for high and intermediate water concentrations, the formation of a micelle and lipid bilayer is always observed using large values of field update interval (up to 900 timesteps) and the grid size (up to $2.5\sigma = 1.175$ nm). Differently, the hexagonal phase expected at low water concentration can be obtained for grid sizes smaller than 2σ ($l \approx 1$ nm) and update interval shorter than 500 timesteps. For larger values of the update interval or of the grid size, the cylinders are not formed and instead irregular reverse micelles are obtained as shown in Fig. 5 (labeled as im).

This behavior can be explained by comparing the size of the grid with the lengthscale of the self-assembling structure. The diameter of the micelle and the bilayer thickness are both about 4 nm, while the diameter of the tubes present in the hexagonal phase is smaller ($\approx$1 nm). Then in this case when the size of the grid used for the density coarse-graining starts to approach the size of the cylindrical tubes, these structures cannot be described correctly. Similar considerations can be made for the density update interval. In Fig. 6 is reported the behavior of the mean square displacement as a function of time for different values of the density update intervals for the two different systems reported in Fig. 2. In particular, in order to compare the displacements with the size of the structures, the square root of the mean square displacement (MSD) normalized by the grid size is reported.

This is a quantitative way to understand the validity of the approximation of slow variation in the field with respect to the particle displacement between two density updates. In fact, the plots shown in Fig. 6 quantify how many cells a particle can cross in a given amount of simulation time. From Fig. 6, it is clear that for update intervals between 500 and 900 steps (corresponding to 15 and 36 ps), both water and DPPC beads undergo a

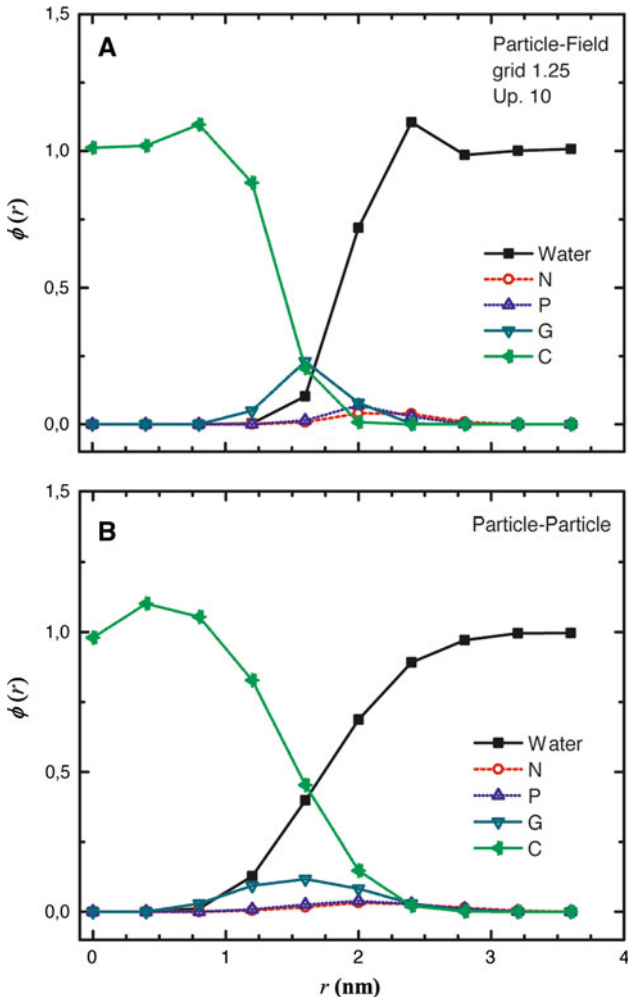

Fig. 3 Radial density profiles of the micelle obtained in the MD-SCF (**a**) and PP (**b**) simulations on system **1**

displacement equal to or larger than a cell size (i.e., larger than 0.6 nm).

From the comparison of the self-assembling processes obtained in the simulations shown in Fig. 2, it is clear that the dynamics of the system simulated in the MD-SCF method is faster than in the PP method. This is due to the smoother potentials and forces characterizing the MD-SCF Hamiltonian. In particular, the models used in the MD-SCF simulation include the effect of excluded volume interactions between particles by using incompressibility condition as described in Eq. 7. Then, forces depend on the derivatives of the density fields with a change much more smoother than distances between particles pairs.

In order to compare more quantitatively the different dynamics in PP and PF models, diffusion coefficients have been calculated from the behavior of the MSD for water and DPPC particles versus time. In particular in Fig. 7, the ratio D^* between diffusion coefficients calculated in the MD-SCF simulations (update interval of 300 timesteps and grid size $l = 2.0\sigma$) and the one calculated in the reference PP simulation is reported. From the figure, it is clear that for all considered systems, the diffusion coefficients calculated in the MD-SCF simulations are always larger than ones calculated in the PP simulations. In particular, for DPPC, they are from 4 to 6 times larger than those in the PP simulations, and for water, they are from 1.25 to 2.5 larger. Absolute values of diffusion coefficients calculated using different grid sizes and update interval for both water and DPPC are reported in Tables 5, 6, 7, 8.

The ratios between the diffusion coefficients obtained in the MD-SCF and PP simulations can be regarded as scaling factors to connect the dynamics of the MD-SCF simulations with that of the reference PP ones. This kind of comparison has been made also for the reference PP simulations to connect their dynamics with atomistic ones [59], and according to this comparison, we can estimate that the reference PP models have a dynamics that is about 4 times faster than atomistic simulations. Considering this point, the dynamics in MD-SCF simulations should be about 20–25 times faster than that in the atomistic simulations. It is interesting to note that the scaling factors between the PP and MD-SCF simulations are functions of water concentrations. In particular, they become larger as the water content becomes smaller. This behavior, from practical purposes, is very convenient because we can simulate with a largely improved efficiency the very slow dynamics in atomistic systems whose equilibration is difficult with the PP coarse-grained or the atomistic simulations.

3.3 Simulations on larger systems

On the basis of the results presented in the previous subsection, MD-SCF simulations on larger systems have been performed using a grid size $l = 1.5\sigma$ and the density update interval of 300 timesteps. In particular, we simulated the spontaneous self-assembling processes in several DPPC/water systems for 1.2 μs using a cubic box with the side lengths that are about double of those used in the simulations reported in the previous subsections. For all considered systems, the starting configuration is made up of randomly mixed lipid and water molecules.

In Fig. 8, the time behaviors of MD-SCF potential together with some snapshots for four DPPC/water systems at different water concentration have been shown (systems **3**–**6**), while the details of these systems are shown in Table 4.

For all of the systems shown in Fig. 8 after 500 ns, the equilibrium is achieved and a stable phase-separated structure is formed. In particular for the system at lower water concentration shown in Fig. 8a (system **3**, 3 water/lipid) after 400 ns, a stable reverse hexagonal phase is formed. At intermediate water content (system **4**, 10 water/

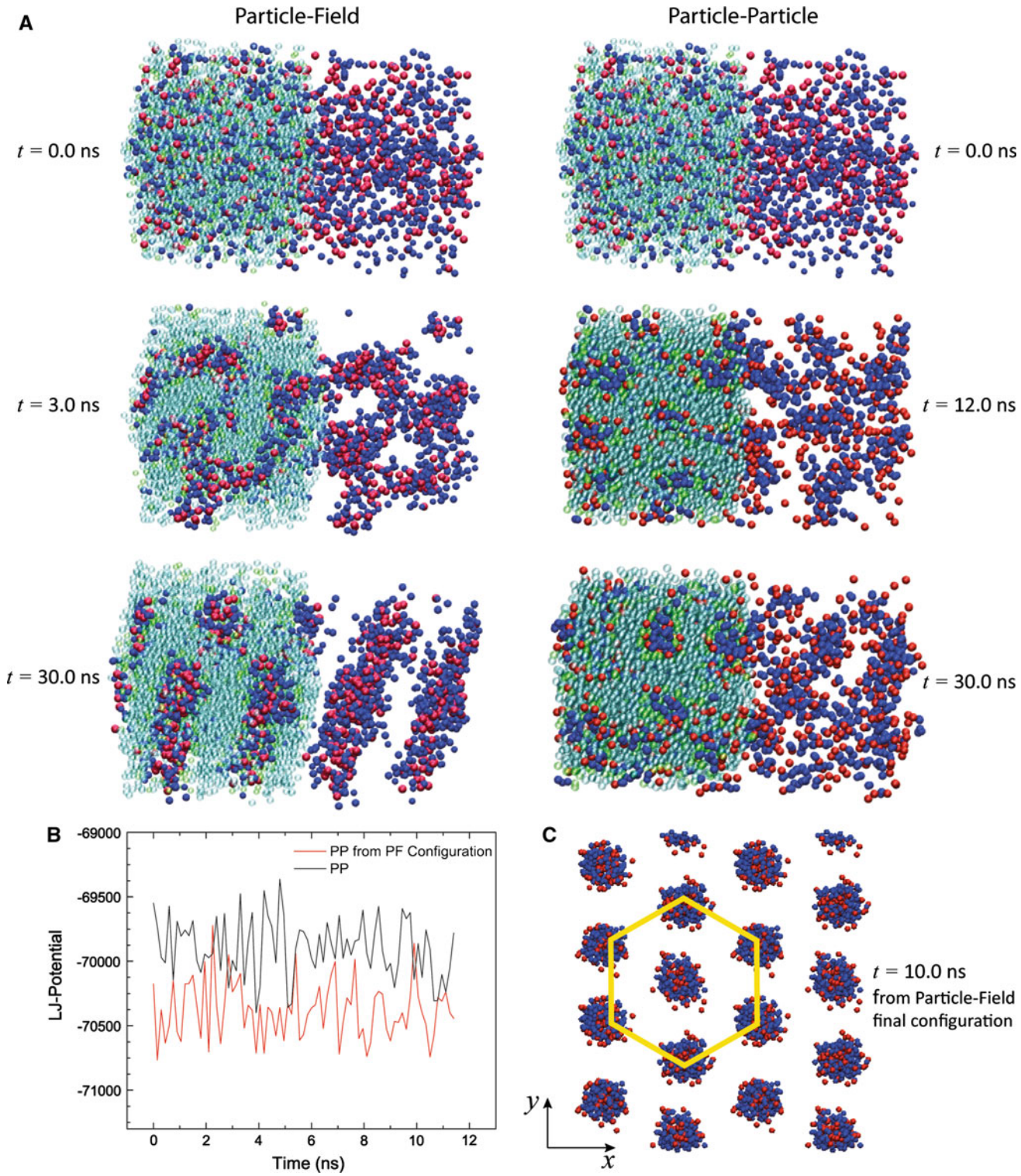

Fig. 4 Comparison of self-assembling process of cylinders in the reverse micellar phase obtained in the MD-SCF and PP simulations (**a**). Comparison between time behavior of Lennard–Jones non-bonded potential (kJ/mol) of PP simulations obtained in a spontaneous assembling process from a uniformly mixed state (*black curve*) and that of PP simulation starting from the self-assembled structure obtained in the MD-SCF simulation (*red curve*) (**b**). Snapshot of the system showing the hexagonal arrangement of cylinders in the reverse micellar phase (**c**)

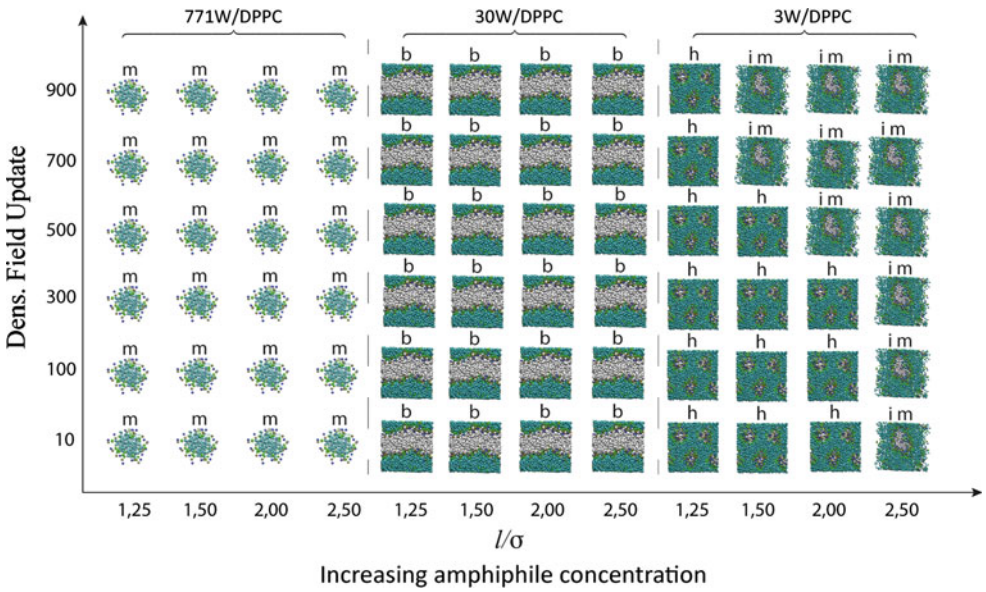

Fig. 5 Graphical matrix summarizing the structures obtained using different density updates intervals (y axis, timesteps unit) and cell sizes l (x axis, unit of σ)

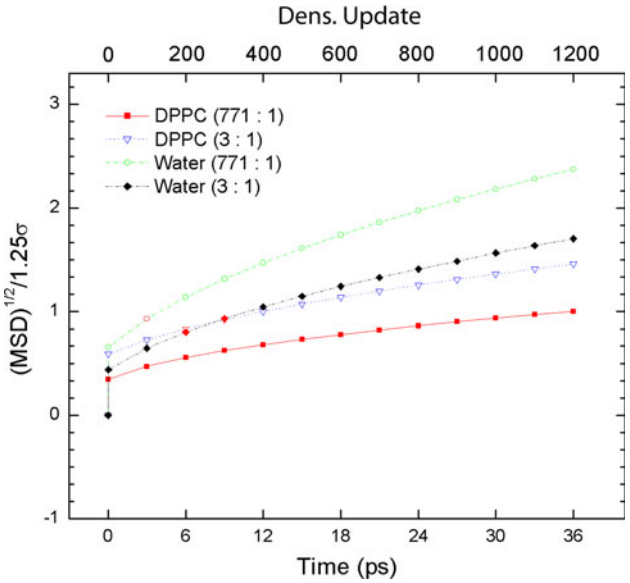

Fig. 6 Square root of normalized mean square displacement of water, DPPC and water beads as a function of time

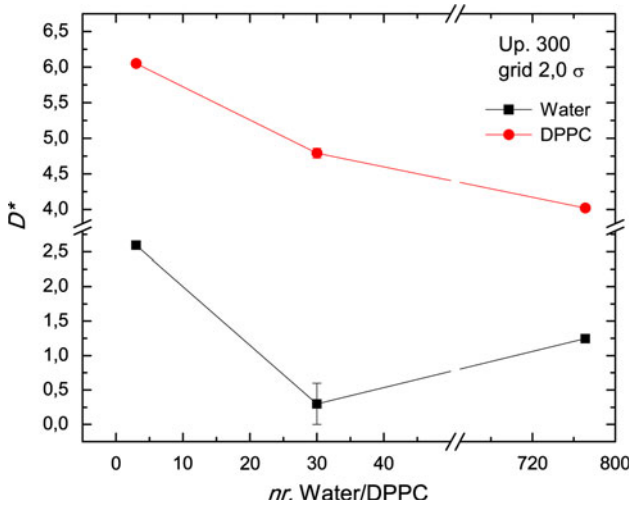

Fig. 7 Ratio between MD-SCF and PP diffusion coefficients as a function of water/DPPC ration calculated for water (*black curve*) and DPPC (*red curve*)

lipid), a stable bilayer phase is formed before 500 ns (Fig. 8b).

Differently, in system **5** (Fig. 8c), where the water content is higher, after a rapid initial local clustering after 100 ns, there is a coalescence to a bilayer structure with curved edges (bicelle) leaving a small single spherical micelle beside it. Between 100 and 200 ns, a process of fusion starts to give a stable bilayer structure with curved edges involving all 300 DPPC molecules present in the simulation box. Finally, the simulation of the system **6** with the water content of 771 water/lipid, after an initial clustering, the formation of two nearly spherical micelles is obtained.

A further validation of the proposed models can be done by considering the average number of lipids/micelle. In the Fig. 9a is reported the time evolution of the number of clusters together with the average number of lipid per cluster for a system having 771 water/lipids. Two lipids are considered to be in the same cluster if at least one distance between their beads is smaller than 1.2 nm. According to this choice, the average number of lipids/cluster (micelle) is about 80. This value has been averaged starting from 400 ns, when the system shows to be in equilibrium. As for available experimental data, sodium dodecyl sulfate (SDS) in physiological conditions forms micelles with an aggregation number ranging from 50 to 80 [64]. In Fig. 9b, the micelle size distribution, averaged from 400 to 600 ns, has

Table 5 Diffusion coefficients calculated using different update intervals and different grid sizes for water in system **1**

Update freq. (timesteps)	Water ($cm^2/s \times 10^5$)			
	$l = 1.25\sigma$	$l = 1.50\sigma$	$l = 2.0\sigma$	$l = 2.5\sigma$
Particle–particle	2.45 ± 0.06	–	–	–
10	3.04 ± 0.06	3.02 ± 0.02	3.04 ± 0.02	2.93 ± 0.07
100	3.06 ± 0.07	3.07 ± 0.01	2.9 ± 0.1	2.94 ± 0.06
300	3.05 ± 0.01	3.12 ± 0.02	3.05 ± 0.05	3.04 ± 0.03
500	3.15 ± 0.03	3.18 ± 0.05	3.08 ± 0.04	3.06 ± 0.01
700	3.23 ± 0.02	3.02 ± 0.05	3.12 ± 0.05	3.08 ± 0.05

Table 6 Diffusion coefficients calculated using different update intervals and different grid sizes for DPPC in system **1**

Update freq. (timesteps)	DPPC ($cm^2/s \times 10^5$)			
	$l = 1.25\ \sigma$	$l = 1.50\ \sigma$	$l = 2.0\ \sigma$	$l = 2.5\ \sigma$
Particle–particle	0.024 ± 0.003	–	–	–
10	0.085 ± 0.004	0.090 ± 0.003	0.132 ± 0.002	0.093 ± 0.001
100	0.12 ± 0.01	0.118 ± 0.008	0.091 ± 0.002	0.992 ± 0.008
300	0.09 ± 0.02	0.12 ± 0.04	0.14 ± 0.05	1.01 ± 0.03
500	0.076 ± 0.004	0.14 ± 0.02	0.089 ± 0.003	1.03 ± 0.03
700	0.089 ± 0.006	0.088 ± 0.003	0.096 ± 0.001	1.14 ± 0.09

Table 7 Diffusion coefficients calculated using different update intervals and different grid sizes for water in system **2**

Update freq. (timesteps)	Water ($cm^2/s \times 10^5$)			
	$l = 1.25\ \sigma$	$l = 1.50\ \sigma$	$l = 2.0\ \sigma$	$l = 2.5\ \sigma$
Particle–particle	0.3813 ± 0.0007	–	–	–
10	1.02 ± 0.06	0.85 ± 0.02	0.98 ± 0.05	1.42 ± 0.02
100	0.957 ± 0.005	0.61 ± 0.08	0.84 ± 0.06	1.61 ± 0.04
300	0.88 ± 0.09	0.90 ± 0.07	0.6 ± 0.3	1.36 ± 0.06
500	0.87 ± 0.08	0.8 ± 0.2	0.859 ± 0.003	1.02 ± 0.04
700	1.07 ± 0.04	0.46 ± 0.03	0.936 ± 0.008	1.340 ± 0.007

Table 8 Diffusion coefficients calculated using different update intervals and different grid sizes for DPPC in system **2**

Update freq. (timesteps)	DPPC ($cm^2/s \times 10^5$)			
	$l = 1.25\ \sigma$	$l = 1.50\ \sigma$	$l = 2.0\ \sigma$	$l = 2.5\ \sigma$
Particle–particle	0.032 ± 0.002	–	–	–
10	0.12 ± 0.01	0.14 ± 0.02	0.20 ± 0.01	0.24 ± 0.05
100	0.132 ± 0.002	0.148 ± 0.004	0.196 ± 0.004	0.24 ± 0.01
300	0.135 ± 0.002	0.155 ± 0.008	0.183 ± 0.001	0.25 ± 0.01
500	0.153 ± 0.007	0.158 ± 0.002	0.16 ± 0.02	0.24 ± 0.01
700	0.16 ± 0.01	0.156 ± 0.003	0.186 ± 0.001	0.25 ± 0.04

been also reported. From the figure, it is clear that the distribution is trimodal, showing three peaks. The first one corresponds to free lipid molecules, the second one corresponds to a smaller micelle composed of about 50 lipids, and the biggest one composed of about 150 lipids. This distribution can be also visualized by looking at some representative simulation snapshot like the one depicted in Fig. 9c. Analogous behavior has been found from PP simulations, where very similar structures can be obtained as shown in Fig. 9c.

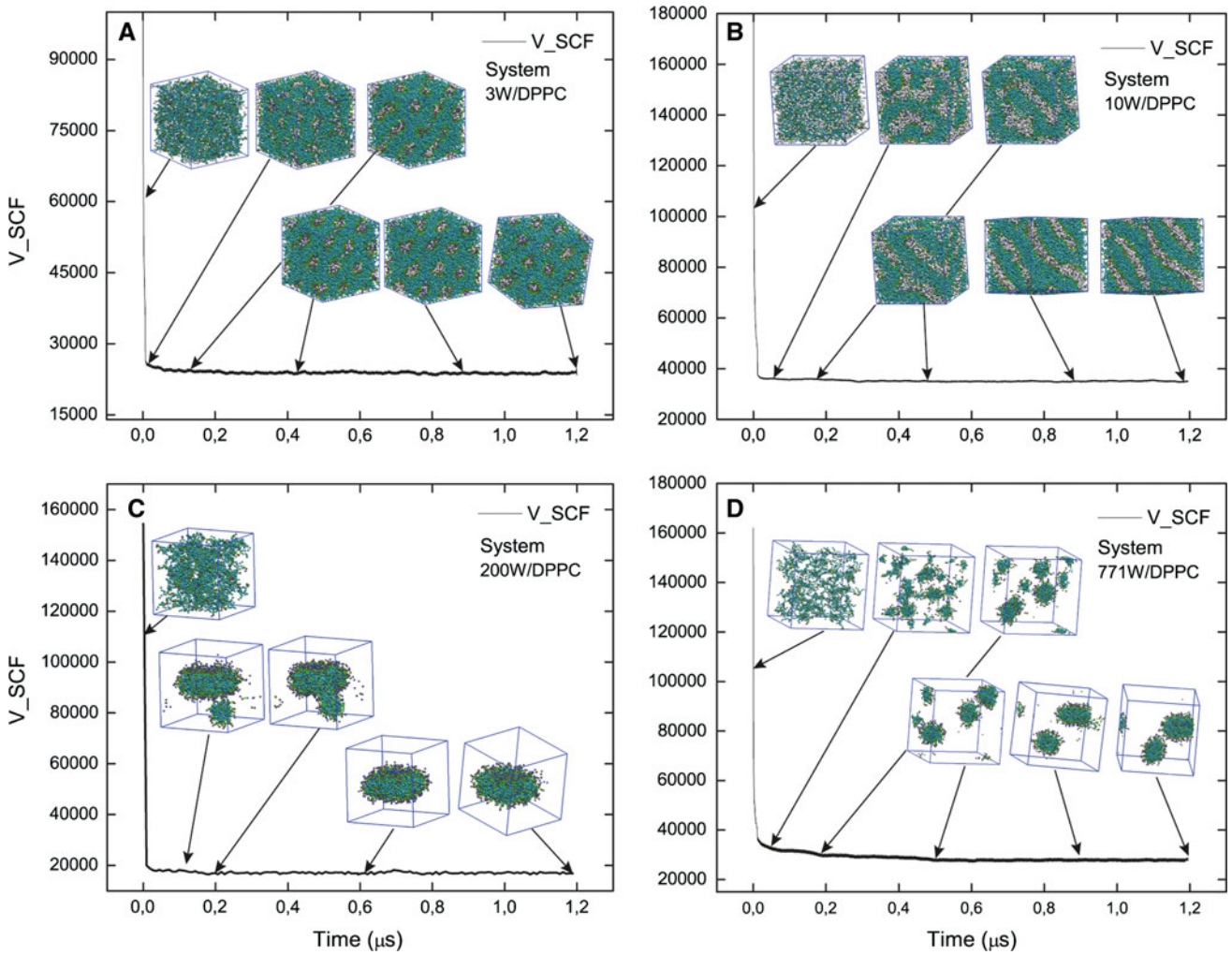

Fig. 8 Time behaviors of the MD-SCF potential together with some snapshots for **a** system **3** forming a reverse micellar hexagonal phase, **b** system **4** forming a lipid bilayer phase, **c** system **5** forming a single bicelle and **d** system **6** forming a micellar phase

4 Conclusions

The validation of a coarse-grained model for phospholipids suitable for a recently developed hybrid methodology combining particles and density fields (MD-SCF) has been reported for DPPC in non-bilayer phases.

According to the mean field coarse-graining strategy, pair interactions between particles are replaced by the calculation of the interactions of single particles in an external field. In principle, the parameters of a coarse-grained model are not always transferable. The comparison between PP and MD-SCF results for non-lamellar phases (stable at low or high water concentration) gave a first confirmation that the proposed models reproduce the correct phase behavior at different compositions. These results encouraged to compare at a more detailed level hybrid particle-field and the reference particle–particle models. In particular, the density profiles of micelles simulated with MD-SCF and conventional MD methods are very similar. Furthermore, the average number of lipids/micelle is well reproduced with respect to reference particle–particle simulations and available experimental data.

As for dynamical properties, the self-assembly process is faster in MD-SCF simulations. Using a systematic comparison between diffusion coefficients, a quantitative scale factors between the dynamics of the coarse-grained hybrid models and the dynamics of corresponding coarse-grained or atomistic particle–particle models have been obtained.

The lower computational costs of the hybrid techniques together with a faster dynamics due to the smoothness of the potentials and forces enable us to perform simulations with a considerably improved efficiency. To have an idea about simulations presented in this paper, for systems **3–6** of Fig. 8, it is possible to calculate about 1 μs/day using 8 processors (Intel E7330, 2.40 GHz). The hybrid MD-SCF

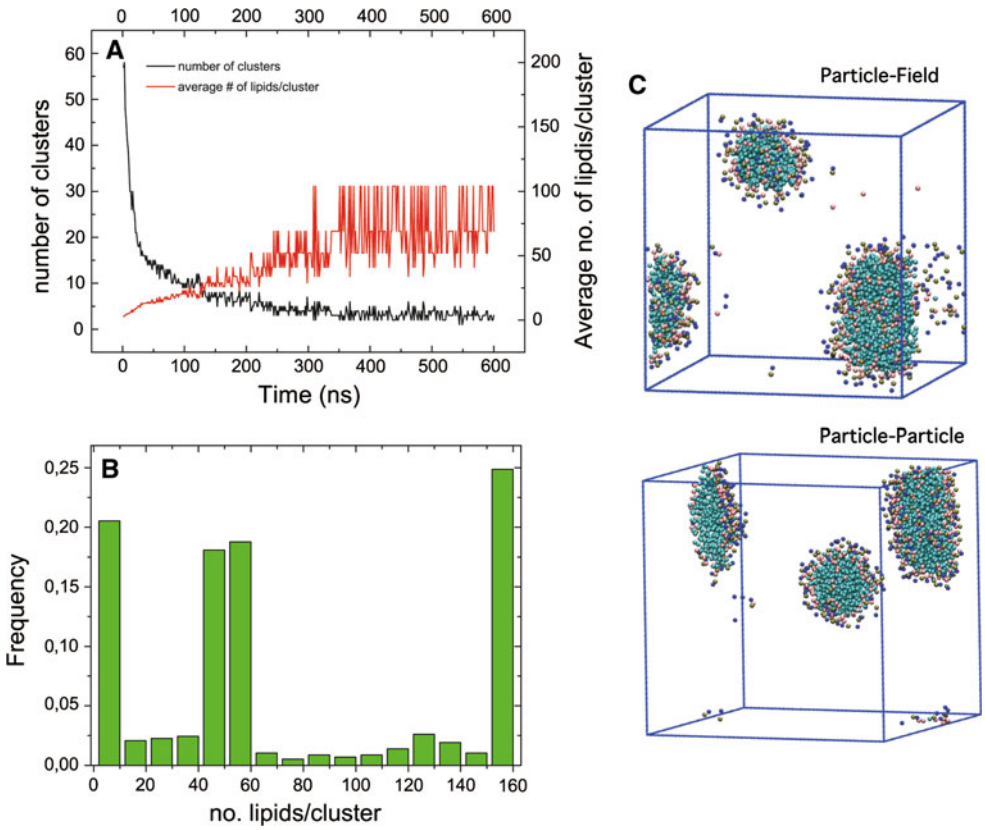

Fig. 9 Time behaviors of number of clusters (*black line*) and average number of lipids per cluster/micelle (*red line*) (**a**). Number of lipids/cluster distribution system (**b**) Snapshots of MD-SCF an PP micellar systems (**c**)

scheme is particularly efficient in parallel simulations, especially for large systems when the use of a large number of CPUs is efficient [61], and the validation of the models presented in this paper will allow their application to large-scale systems needed to study the application of the self-assembled structures of lipids to nanotechnologies.

Acknowledgments This paper is dedicated to Vincenzo Barone for his 60th birthday. G. M. is particularly beholden to Vincenzo who drove his first steps into the fascinating world of theoretical chemistry. G. M. thanks MIUR (PRIN2008 and FIRB "RETE ITALNANONET") for financial support and the HPC team of Enea (http://www.enea.it) for using the ENEA-GRID and the HPC facilities CRESCO (http://www.cresco.enea.it) in Portici, Italy. D. R. and G. M. thank Deutschen Forschungsgemeinschaft (DFG) for funding in the framework of the project "*The study of detailed mechanism of polymers/biological membrane interactions using computer simulation*" (RO 3571/3-1). T. K. thanks the Grant-in-Aid for Science from the Ministry of Education, Culture, Sports, Science and Technology, Japan on the Priority Area "Soft Matter Physics".

References

1. Bandyopadhyay S, Tarek M, Klein ML (1999) Molecular dynamics study of a lipid-DNA complex. J Phys Chem B 103(46):10075–10080. doi:10.1021/jp9927496
2. Saiz L, Klein ML (2002) Computer simulation studies of model biological membranes. Acc Chem Res 35(6):482–489. doi:10.1021/ar010167c
3. Faller R, Marrink S-J (2004) Simulation of domain formation in DLPC-DSPC mixed bilayers. Langmuir 20(18):7686–7693. doi:10.1021/la0492759
4. Pal S, Milano G, Roccatano D (2006) Synthetic polymers and biomembranes. How do they interact?: Atomistic molecular dynamics simulation study of PEO in contact with a DMPC lipid bilayer. J Phys Chem B 110(51):26170–26179. doi:10.1021/jp063418d
5. Bennett WFD, MacCallum JL, Hinner MJ, Marrink SJ, Tieleman DP (2009) Molecular view of cholesterol flip-flop and chemical potential in different membrane environments. J Am Chem Soc 131(35):12714–12720. doi:10.1021/ja903529f
6. Katsaras J, Tristram-Nagle S, Liu Y, Headrick RL, Fontes E, Mason PC, Nagle JF (2000) Revisiting the ripple phase using fully hydrated, aligned DPPC multibilayers. Biophys J 78(1):20A
7. Ayton G, Smondyrev AM, Bardenhagen SG, McMurtry P, Voth GA (2002) Calculating the bulk modulus for a lipid bilayer with non-equilibrium molecular dynamics simulation. Biophys J 82:1226–1238
8. Ayton G, Voth GA (2004) Mesoscopic lateral diffusion in lipid bilayers. Biophys J 87(5):3299–3311
9. Ayton G, Voth GA (2007) Multiscale simulation of transmembrane proteins. J Struct Biol 157(3):570–578
10. Gurtovenko AA, Anwar J, Vattulainen I (2010) Defect-mediated trafficking across cell membranes: insights from in silico modeling. Chem Rev 110(10):6077–6103. doi:10.1021/cr1000783
11. Izvekov S, Voth GA (2006) Multiscale coarse-graining of mixed phospholipid/cholesterol bilayers. J Chem Theory Comput 2(3):637–648. doi:10.1021/ct050300c
12. Shi Q, Voth GA (2005) Multi-scale modeling of phase separation in mixed lipid bilayers. Biophys J 89(4):2385–2394
13. Tepper HL, Voth GA (2006) Mechanisms of passive ion permeation through lipid bilayers: insights from simulations. J Phys Chem B 110(42):21327–21337. doi:10.1021/jp064192h
14. Venturoli M, Sperotto MM, Kranenburg M, Smit B (2006) Mesoscopic models of biological membranes. Phys Rep Rev Sect Phys Lett 437(1–2):1–54. doi:10.1016/j.physrep.2006.07.006

15. Marrink SJ, de Vries AH, Tieleman DP (2009) Lipids on the move: simulations of membrane pores, domains, stalks and curves. Biochim Biophys Acta 1788(1):149–168. doi:10.1016/j.bbamem.2008.10.006
16. Psachoulia E, Marshall DP, Sansom MSP (2010) Molecular dynamics simulations of the dimerization of transmembrane alpha-helices. Acc Chem Res 43(3):388–396. doi:10.1021/ar900211k
17. Lyubartsev AP, Rabinovich AL (2011) Recent development in computer simulations of lipid bilayers. Soft Matter 7(1):25–39. doi:10.1039/c0sm00457j
18. Burkett SL, Mann S (1996) Spatial organization and patterning of gold nanoparticles on self-assembled biolipid tubular templates. Chem Commun 3:321–322
19. Bhattacharya S, Srivastava A (2003) Synthesis and characterization of novel cationic lipid and cholesterol-coated gold nanoparticles and their interactions with dipalmitoylphosphatidylcholine membranes. Langmuir 19(10):4439–4447. doi:10.1021/la0269513
20. Wallace EJ, Sansom MSP (2009) Carbon nanotube self-assembly with lipids and detergent: a molecular dynamics study. Nanotechnology 20(4):045101. doi:10.1088/0957-4484/20/4/045101
21. Lian T, Ho RJY (2001) Trends and developments in liposome drug delivery systems. J Pharm Sci 90(6):667–680
22. Bolinger PY, Stamou D, Vogel H (2004) Integrated nanoreactor systems: triggering the release and mixing of compounds inside single vesicles. J Am Chem Soc 126(28):8594–8595. doi:10.1021/ja049023u
23. Jang J, Yoon H (2005) Formation mechanism of conducting polypyrrole nanotubes in reverse micelle systems. Langmuir 21(24):11484–11489. doi:10.1021/la051447u
24. Müller M, Katsov K, Schick M (2006) Biological and synthetic membranes: what can be learned from a coarse-grained description? Phys Rep 434(5–6):113–176
25. Sintes T, Baumgaertner A (1998) Interaction of wedge-shaped proteins in flat bilayer membranes. J Phys Chem B 102(36):7050–7057
26. Lenz O, Schmid F (2005) A simple computer model for liquid lipid bilayers. J Mol Liq 117(1–3):147–152. doi:10.1016/j.molliq.2004.08.008
27. Marrink SJ, de Vries AH, Mark AE (2003) Coarse grained model for semiquantitative lipid simulations. J Phys Chem B 108(2):750–760. doi:10.1021/jp036508g
28. Marrink S-J, Mark AE (2004) Molecular view of hexagonal phase formation in phospholipid membranes. Biophys J 87(6):3894–3900
29. Marrink SJ, Mark AE (2003) The mechanism of vesicle fusion as revealed by molecular dynamics simulations. J Am Chem Soc 125(37):11144–11145. doi:10.1021/ja036138+
30. Kawakatsu T (2004) Statistical physics of polymers. Springer, Berlin
31. Matsen MW, Schick M (1994) Stable and unstable phases of a diblock copolymer melt. Phys Rev Lett 72(16):2660–2663
32. Drolet F, Fredrickson GH (1999) Combinatorial screening of complex block copolymer assembly with self-consistent field theory. Phys Rev Lett 83(21):4317–4320
33. Fredrickson GH, Ganesan V, Drolet F (2002) Field-theoretic computer simulation methods for polymers and complex fluids. Macromolecules 35(1):16–39. doi:10.1021/ma011515t
34. Lauw Y, Leermakers FAM, Stuart MAC (2006) Self-consistent-field analysis of the micellization of carboxy-modified poly(ethylene oxide)-poly(propylene oxide)-poly(ethylene oxide) triblock copolymers. J Phys Chem B 110(1):465–477
35. Ly DQ, Honda T, Kawakatsu T, Zvelindovsky AV (2008) Hexagonally perforated lamella-to-cylinder transition in a diblock copolymer thin film under an electric field. Macromolecules 41(12):4501–4505
36. Dickinson E, Pinfield VJ, Home DS, Leermakers FAM (1997) Self-consistent-field modelling of adsorbed casein interaction between two protein-coated surfaces. J Chem Soc, Faraday Trans 93(9):1785–1790
37. Balazs AC, Singh C, Zhulina E (1998) Modeling the interactions between polymers and clay surfaces through self-consistent field theory. Macromolecules 31(23):8370–8381
38. Roan JR, Kawakatsu T (2002) Self-consistent-field theory for interacting polymeric assemblies. I. Formulation, implementation, and benchmark tests. J Chem Phys 116(16):7283–7294
39. Roan JR, Kawakatsu T (2002) Self-consistent-field theory for interacting polymeric assemblies. II. Steric stabilization of colloidal particles. J Chem Phys 116(16):7295–7310
40. Marcelja S (1973) Molecular model for phase transition in biological membranes. Nature 241(5390):451–453
41. Leermakers FAM, Rabinovich AL, Balabaev NK (2003) Self-consistent-field modeling of hydrated unsaturated lipid bilayers in the liquid-crystal phase and comparison to molecular dynamics simulations. Phys Rev E 67(1):011910
42. Leermakers FAM, Scheutjens J (1988) Statistical thermodynamics of association colloids. 1. Lipid bilayer-membranes. J Chem Phys 89(5):3264–3274
43. Ayton G, McWhirter JL, Voth GA (2006) A second generation mesoscopic lipid bilayer model: connections to field-theory descriptions of membranes and nonlocal hydrodynamics. J Chem Phys 124(6):12. doi:10.1063/1.2165194
44. Muller M, Smith GD (2005) Phase separation in binary mixtures containing polymers: a quantitative comparison of single-chain-in-mean-field simulations and computer simulations of the corresponding multichain systems. J Polym Sci, Part B: Polym Phys 43(8):934–958
45. Daoulas KC, Muller M, Stoykovich MP, Park SM, Papakonstantopoulos YJ, de Pablo JJ, Nealey PF, Solak HH (2006) Fabrication of complex three-dimensional nanostructures from self-assembling block copolymer materials on two-dimensional chemically patterned templates with mismatched symmetry. Phys Rev Lett 96(3):036104
46. Detcheverry FA, Kang HM, Daoulas KC, Muller M, Nealey PF, de Pablo JJ (2008) Monte Carlo simulations of a coarse grain model for block copolymers and nanocomposites. Macromolecules 41(13):4989–5001
47. Detcheverry FA, Pike DQ, Nealey PF, Müller M, de Pablo J (2010) Simulations of theoretically informed coarse grain models of polymeric systems. Faraday Discuss 144:111–125
48. Milano G, Kawakatsu T (2009) Hybrid particle-field molecular dynamics simulations for dense polymer systems. J Chem Phys 130(21):214106
49. Milano G, Kawakatsu T (2010) Pressure calculation in hybrid particle-field simulations. J Chem Phys 133(21):214102. doi:10.1063/1.3506776
50. De Nicola A, Zhao Y, Kawakatsu T, Roccatano D, Milano G (2011) Hybrid particle-field coarse-grained models for biological phospholipids. J Chem Theory Comput 7(9):2947
51. Schmid F (1998) Self-consistent-field theories for complex fluids. J Phys: Condens Matter 10(37):8105–8138. doi:10.1088/0953-8984/10/37/002
52. Matsen MW (2002) The standard Gaussian model for block copolymer melts. J Phys Condens Matter 14(2):R21. doi:10.1088/0953-8984/14/2/201
53. Fredrickson GH (2005) The equilibrium theory of inhomogeneous polymers, vol 1. Oxford University Press, Oxford
54. Helfand E, Tagami J (1972) Theory of the interface between immiscible polymers. II. J Chem Phys 56(7):10. doi:10.1063/1.1677735
55. Eastwood JW, Hockney RW, Lawrence DN (1980) P3M3DP—the three-dimensional periodic particle–particle/particle-mesh program. Comput Phys Commun 19(2):215

56. Deserno M, Holm C (1998) How to mesh up Ewald sums. I. A theoretical and numerical comparison of various particle mesh routines. J Chem Phys 109(12):7678
57. Norizoe Y, Daoulas KC, Muller M (2010) Measuring excess free energies of self-assembled membrane structures. Faraday Discuss 144:369–391
58. Daoulas KC, Muller M (2006) Single chain in mean field simulations: Quasi-instantaneous field approximation and quantitative comparison with Monte Carlo simulations. J Chem Phys 125(18):184904
59. Marrink S-J, Risselada HJ, Yefimov S, Tieleman DP, de Vries AH (2007) The MARTINI force field: coarse grained model for biomolecular simulations. J Phys Chem B 111(27):7812–7824. doi:10.1021/jp071097f
60. Van der Spoel D, Lindahl E, Hess B, Groenhof G, Mark AE, Berendsen HJC (2005) GROMACS: fast, flexible, and free. J Comput Chem 26(16):1701–1718
61. Zhao Y, De Nicola A, Kawakatsu T, Milano G (2012) Hybrid particle-field molecular dynamics simulations: parallelization and benchmarks. J Comput Chem 33:868–880. doi:10.1002/jcc.22883
62. Carbone P, Varzaneh HAK, Chen X, Muller-Plathe F (2008) Transferability of coarse-grained force fields: the polymer case. J Chem Phys 128(6):064904–064911
63. Tuckerman ME, Glenn JM, Bruce JB (1990) Molecular dynamics algorithm for condensed systems with multiple time scales. J Chem Phys 93(2):5. doi:10.1063/1.459140
64. Moroi Y (1992) Micelles. Theoretical and applied aspects. Springer, Berlin